Paper No.
04598

CORROSION2004

STUDIES ON THE CORROSION BEHAVIOR OF STAINLESS STEELS IN CHLORIDE SOLUTIONS IN THE PRESENCE OF SULFATE REDUCING BACTERIA

Lietai Yang and Gustavo A. Cragnolino
Center for Nuclear Waste Regulatory Analyses
Southwest Research Institute
6220 Culebra Rd
San Antonio, TX 78238

ABSTRACT

Experimental studies on the corrosion of Types 304 and 304L stainless steels (SS) in 0.5M chloride solutions with the presence of sulfate reducing bacteria (SRB) and a slime former were conducted. Coupled multielectrode sensors and electrochemical polarization techniques were employed in this study. No significant difference between the repassivation potentials was observed with and without the presence of SRB. The SS electrodes in both the SRB-containing and the SRB-free solutions were coupled to large SS cathodes in a separate aerated cell and their potentials were increased stepwise from –0.26 to –0.04 V_{SCE}. No pitting was observed on the electrodes after three-month exposure. Anodic polarization measurements using a platinum electrode in the SRB-containing solution suggest that the anodic peak observed on the SS electrode was probably due to the oxidation of reducing species and attached to the electrode surface by the SRB. It was concluded that use of the anodic current density to characterize microbially induced corrosion of metals might lead to wrong interpretation.

Keywords: microbiologically influenced corrosion, MIC; sulfate reducing bacteria, SRB; stainless steel, multielectrode sensor, coupled multielectrode sensor

INTRODUCTION

Microbially influenced corrosion (MIC) is known as a problem affecting metallic materials used in many industries including power generation, oil and gas production and transmission, and chemical processing among others, and in many cases affecting cooling water systems.[1] There have been concerns regarding MIC in nuclear waste disposal[2,3] and the potential for MIC in the specific case of a potential high level radioactive waste repository at Yucca Mountain.[4]

The material selected by the U.S. Department of Energy[5] for the outer container of the waste package for a potential repository at Yucca Mountain is a Ni-Cr-Mo-W alloy, Alloy 22 (UNS N06022). This alloy is considered to be highly resistant to corrosion in the aqueous environments expected in the waste emplacement drifts after the dry-out period.[6] However, its resistance to MIC is still a matter of concern.[7] As part of an effort to evaluate the potential susceptibility of Alloy 22 to MIC, this work is a preliminary study on MIC aimed to select a suitable environment and a proper consortium of microorganisms known or anticipated to exist at Yucca Mountain for

further testing. The primary objective of this study is to evaluate the applicability of several electrochemical techniques to investigate the susceptibility of Alloy 22 to MIC. Because the rate of MIC of Alloy 22 is very low, Types 304 and 304L SS were selected as appropriate alloys for the purpose of evaluating the techniques and sulfate reducing bacteria (SRB) as surrogate microorganisms for those existing in Yucca Mountain.

EXPERIMENTAL APPROACH

Experimental Setup

It was previously reported[8] that the corrosion rate of Type 304 SS was very low in deaerated 0.5 M NaCl solutions in the presence of SRB and slime former. The lack of corrosion was attributed to the low electrochemical potential of the SS specimen in the deaerated solution. In the usual practice, SS components exposed to the SRB-thriving conditions are electrically connected to the other sections or other components that are exposed to oxygen-rich or other oxidizing environments. Hence the potential of the SS components are higher. To mimic this condition, SS sensors and SS electrodes in a continuously deaerated test cell were coupled to separate large SS cathodes in an aerated cell (Figure 1). Both cells were filled with 500 mL 0.5M NaCl solution that was prepared with reagent grade chemicals and de-ionized water {18 Mohm-cm [7.1 Mohm-in] resistivity}. A salt bridge filled with the same solution connected the two cells. The test cell contained a slime former *(Vibrio natriegens* ATCC[(1)] 14048) grown in 1.5 percent NaCl nutrient broth (Table 1) and an SRB (*Desulfovibrio vulgaris* ATCC 29579) grown in a modified Baar's Broth medium (Table 2) both from Anaerobe System, Morgan Hill, California. The slime former (10 mL in 1.5 percent NaCl nutrient broth) and sterile modified Baar's Broth medium (30 mL) were added at the beginning of each test. Initial inoculation of organism into the test system was performed by growing each of the organisms in selective media for an incubation period aimed to achieving log phase growth that is active growth of each organism type. The *Vibrio natriegens* was grown in the 1.5 percent nutrient broth at 31 ± 1˚C (87.8 ± 1.8˚F) for approximately 4 hours to achieve a log phase growth. The SRB was incubated for 48 hours under the same temperature conditions but in an anaerobic environment (Bio Bag Type A, from Becton Dickinson, Franklin Lakes, New Jersey) using modified Baar's Broth medium to achieve a log phase growth. The SRB (10 mL in modified Baar's Broth) was introduced into the test cell about 7 days after the addition of the slime former. A third cell, identical to the test cell, was used as a control cell. The same amount of slime former, and modified Baar's Broth medium was added to the control cell each time they were added to the test cell. To maintain the growth of the SRB and the slime former, 10 mL sterile Baar's Broth medium was added to the test and control cells approximately every 35 hours during the entire test period. Harvest samples of approximately 10 mL each from the two cells were taken on a regular basis and cultured for the population counts of both SRB and slime former using standard serial dilution technique. The cell density of the slime former was maintained at 10^5 to 10^{10} cfu (colony forming units)/mL in the two cells and no SRB was found in the control cell through out the test.

Reference electrodes, platinum electrodes and duplicate Types 304 and 304L SS electrodes were placed in the three cells for polarization and repassivation measurements. The currents flowing from the SS electrodes in both the test and the control cells to the large SS cathodes in the aerated cell were measured by the voltage drops across the resistors as shown in Figure 1. All tests were conducted at room temperature {about 24°C [75.2°F]}.

Coupled Multielectrode Array Sensor

The operating principle and the high-resolution current-measuring system for the coupled multielectrode sensors have been described elsewhere.[9–11] In our previous studies, the sensing electrodes were imbedded in an insulating material; usually epoxy, and only the cross sections of the electrodes at the tip were exposed to the electrolyte of interest and served as the sensing surface. In several cases, however, crevice corrosion was noted in the interface between the sensing electrode and the epoxy in sensors made of corrosion-resistant alloys exposed to highly corrosive solutions. To avoid possible crevice effects on the measurement, crevice-free multielectrode sensors (Figure 2) were used in this study. Approximately 3 cm [1.18 in] of a sensing electrode protruded from

[(1)]ATCC-American Type Culture Collection.

the epoxy and only a portion of the length at the tip was immersed in solution during the test, maintaining the area potentially susceptible to crevice corrosion away from the solution during the measurement. The sensing electrodes of the sensors were made of Type 304 SS. Each sensor had 16 sensing electrodes cut from 1 mm [0.039 in] diameter wires {0.102 cm^2 [0.0158 in^2]} immersed electrode area. The chemical composition of the SS is listed in Table 3. A total of two Type 304 SS sensors were used in this study. Before each test, the sensing surface of the sensors were polished with 600-grit silicon carbide (SiC) paper and cleaned with acetone.

Stainless Steel Electrodes and Polarization Measurements

Two types of SS electrodes were used. One was made of Type 304L SS plate with a dimension of 1.27 cm [0.5 in] in width, 5.08 cm [2 in] in length and 0.21 cm [0.0827 in] in thickness (referred as SS plate electrode). The other type was made of Type 304 SS wire (same wire as mentioned for the coupled multielectrode array sensors, referred to as SS wire electrode). The composition of the Type 304L SS is given in Table 3. The immersion depth of the plate and the wire electrodes was such that their effective surface areas were approximately 3.2 cm^2 [0.496 in^2]. All surfaces of the plate and wire electrodes were polished with 600-grit SiC paper and cleaned with acetone before the experiment. No re-cleaning or repolishing was performed during the experiments due to the difficulties in maintaining the anaerobic environment.

The large cathodes shown in Figure 1 were 1-mm- [0.039-in-] diameter SS coils made from the same wire used for the multielectrode array sensors. The surface areas of the cathodes were approximately 94.2 cm^2 [14.6 in^2]. The cathode-to-anode surface area ratios were 57.7 and 14.7 for the sensor electrodes and the plate or the wire electrodes respectively.

A potentiostat (Model 1287A, from Solartron, UK) and the associated controlling software (CorrWare, version 2.2, from Scribner Associates, Southern Pines, North Carolina) were used for the electrochemical measurements. All cyclic potentiodynamic polarization (CPP) tests were conducted at a scan rate of 0.1667 mV/s.

Repassivation potential is defined as the lowest potential at which pitting corrosion may occur. The repassivation potential was determined using the method similar to the one described by Akashi et al.[12] The electrode was potentiodynamically scanned from the open circuit steady-state potential toward the more noble direction at a rate of 0.5 mV/s. As soon as the anodic current reached 0.2 mA, which indicates the initiation and propagation of pitting corrosion, the current was galvanostatically held at 0.2 mA to allow further propagation of pitting corrosion for 2 hours. Subsequently the electrode was potentiodynamically scanned toward the less noble direction at a rate of 0.167 mV/s until the current reached 0.05 mA and held the potential constant for 2 hours. If the current was higher than 1×10^{-6} A/cm^2 at the end of the 2-hour hold, suggesting continued propagation of pitting corrosion, the potential was lowered by 10 mV and held constant for another 2 hours. If the current was still higher than 1×10^{-6} A/cm^2 at the end of the second 2-hour hold, the potential was lowered by another 10 mV and held for 2 hours. This step was repeated until the current remained below 1×10^{-6} A/cm^2 at the end of each 2-hour hold, suggesting no more active pitting corrosion.

RESULTS

Signals from the Multielectrode Array Sensors and Galvanic Currents from SS Electrodes

Figure 3 presents the SRB growth in the test cell, the non-uniform currents and the potential of the sensors in both the test and the control cells during the first month measurement of a three-month test. The SRB in the test cell increased rapidly to 10^{10}cfu/ml shortly after the inoculation and was maintained at about 10^8 cfu/ml during the experiment. However, the signals from the two sensors were about the same and both were relatively low, suggesting little localized corrosion activity on the Type 304 SS sensing electrodes in the two cells. The potential of the sensing electrodes during this period was between –0.16 and –0.26 V_{SCE}, which was below the repassivation potential measured during this study (see next section). The potential decreased with time slowly. This trend was partly due to the increase of pH in the aerated cell from about 6.2 at the beginning of the test to 10.3 three months after (Figure 3 shows only the first month of the results). The coupling of the sensing electrodes

to the relatively large SS-wire cathode in the aerated cell was not effective in raising the potential of the sensing electrodes in both the test and the control cells.

The open circuit steady-state potential of the Type 304 SS in the aerated cell filled with pure NaCl solution was between –0.03 to –0.15 V_{SCE} (see next Section). However, its potential dropped by more than 0.10 V after the connection with the small SS sensing electrodes in the deaerated cells even though the cathode-to-anode surface area ratio was 67. The significant decrease of the potential of the cathode was probably due to the poor kinetics of the oxygen-reduction reaction on the SS cathode in the air-saturated sodium chloride solution at room temperature.

Figure 4 presents the coupling potential and the galvanic currents from the Type 304L SS plate electrodes in both the test and the control cells to a separate SS cathode in the aerated cell (see Figure 1). Similarly to the behavior exhibited by the sensors, the coupling potential of the SS plate electrodes was also low (–0.16 to –0.26 V_{SCE}) and below the repassivation potential (see next section). The anodic galvanic current from the SS plate electrode in the test cell was slightly higher than that from the control cell. No pitting corrosion took place as confirmed by the optical examination of the electrode at the end of the experiment.

Usually, the water containing SRB contains other chemical species such as manganese and iron. It may also contain other microorganisms such as iron-or manganese-oxidizing bacteria.[13–14] The presence of oxidizing microorganisms and/or oxidizing chemical species may cause the ennoblement of SS in solutions.[15] For example, open circuit potential values over 0.3 V_{SCE} have been widely reported for SS in sea water.[16] Figure 5 shows the responses of the coupling potentials of both the sensing electrodes and the SS plate electrodes to the addition of 1 mM H_2O_2 that may be produced by iron- or manganese-oxidizing bacteria in a natural environment[15] and 1 mM $FeCl_2$. In both cases, the electrodes were ennobled by more than 0.30 V. The ennoblement by $FeCl_2$ decreased to approximately 0.1 V above the previous value over a two-day period. The decrease was probably due to the precipitation of solids observed at the bottom of the aerated cell.

To simulate the ennoblement of the large cathodes in the aerated cell, a battery was connected in series in each of the cathode-anode circuits as shown in Figure 1. The battery output could be adjusted to change the values of the coupling potential. Figure 6 shows the response of the signals from the sensors to the changes of the coupling potential. The potential was held at approximately –0.25 V_{SCE} for 16 days, –0.15 V_{SCE} for 12 days, and –0.05 V_{SCE} for 21 days. The current signals from the sensors in both the test and in the control cells increased with the increase of the potential and returned to approximately the previous values after the battery was removed near the end of the test. As the potential was lower than the pit initiation potential (see next section) and not definitively higher than the repassivation potential (–0.15 to –0.03 V_{SCE}) for a considerable length of time, no significant increase in the sensor signals was observed. This is in agreement with the post-test examination that showed no pit on the surface of the sensing electrodes of the sensors after the test. Figure 6 also shows that there was no significant difference between the current signals from the two sensors (i.e., the Type 304 SS sensing electrodes exhibited the absence of localized corrosion both in the SRB cell and in the control cell). This is in agreement with the measured repassivation potentials that indicate no difference between the two environments (see next section).

Figure 7 shows the responses of the galvanic coupling currents from the two Type 304L SS plate electrodes to the change of potential during the same test period as indicated in Figure 6. The potential was held at approximately –0.235 V_{SCE} for 16 days, –0.12 V_{SCE} for 12 days, and –0.04 V_{SCE} for 21 days. In general, the anodic galvanic coupling currents from the plate electrodes increased with the increase of potential. In general, the anodic coupling current from the electrode in the test cell was higher than that in the control cell. Figure 8 shows that the SRB increased rapidly to 10^8 cfu/mL about 10 days after the inoculation and remained at about 10^8 mL after the initial growth by the addition of the medium approximately every 35 hrs on average until June 26, 2003. Because the medium was not available and the regular addition was stopped on June 26, 2003, the growth of SRB decreased and reached 10^4 cfu/mL on July 8, 2003. Then the regular addition of the medium was resumed and the growth of SRB increased. The SRB was maintained at approximately 10^6 cfu/mL until the end of the test. Figure 8 seems to show that the galvanic coupling current from the plate electrode in the test cell correlates with

the SRB density except at the very beginning of the test. The anodic galvanic coupling current was high when the SRB density was over 10^8cfu/mL, but decreased when the SRB density decreased to about 10^4 cfu/mL and remained low during the latter stage of the test when the SRB density was about 10^6 cfu/mL. If the galvanic coupling current was due to the anodic dissolution of the SS plate electrode, Figure 8 suggests that SRB seem to promote a higher corrosion rate for the Type 304L SS.

As in the case of the Type 304 SS sensor electrodes, post-test examination on the Type 304L SS plate electrode showed no pit on the surface after the test. This result is in agreement with the measurements of pit initiation and repassivation potentials because the potential of the Type 304L SS plate electrodes did not lay between the pit initiation potential (see next section) and the repassivation potential (+0.06 to –0.065 V_{SCE}, see next section) for a time sufficient to initiate pitting corrosion.

Repassivation and Cyclic Potentiodynamic Polarization Behaviors

Typical cyclic potentiodynamic polarization (CPP) curves for Types 304 and 304L SS are presented in Figure 9. The curves for both the control and the aerated cells are typical of all the results obtained through out the testing period, while the curve for the test cell was only obtained when the SRB density was high. In addition, the curve for the control cell is identical to that from the aerated cell, suggesting that the slime former and the media which contain a wide range of added chemical components (see Tables 1and 2) in the control cell had little effect on the anodic behavior of SS. However, the typical CPP curve obtained in the test cell when the SRB density was high is significantly different. It has a distinctive anodic peak at a potential near the repassivation potential (corresponds to the potential at which the current decreased dramatically to below 1×10^{-6} A/cm^2 in Figure 9 during a reversed potentiodynamic scan) and exhibited a high current density in the passive region. The characteristic parameters of the curves from both the CPP and the repassivation potential measurements are as follows:

Repassivation Potential. Figure 10 shows the repassivation potentials obtained in the three cells for the two types of SS electrodes at different times during the test period of three months. The repassivation potentials are all between –0.01 to –0.15 V_{SCE} for the Type 304 SS and between +0.06 to –0.065 V_{SCE} for the Type 304L SS in all the cells (test, control and aerated). The repassivation potential remained unchanged during the course of the test even though the pH of all solutions increased. For example, the solution in the aerated cell changed from pH=6.2 at the beginning of the test to pH=10.33 at the end of the test. In addition, the repassivation potential measured in the test cell was found to be independent of the SRB density in the solution (see also Figure 8) for both SS. The scattering of the measured repassivation potential data shown in Figure 10 is typical for passive alloys.

Pit Initiation Potential. Pit initiation potential has been widely used as an indicator of the resistance to localized corrosion. Figure 11 shows the pit initiation potentials obtained in the different cells for the two types of SS electrodes during the experiment. The pit initiation potentials are scattered in a wide range (0.1 to 0.6 V_{SCE}). However, in most cases, the values obtained from the test cell are lower than those obtained from both the aerated and the control cells for the two types of SS. Most of the values from the test cell lie close to 0.15 V_{SCE}. There is one exceptional low value (0.145 V_{SCE}) measured from the aerated cell (Figure 11b), which cannot be explained. No apparent correlation between the SRB density (see Figure 8) and the pit initiation potential of the SS electrodes can be drawn from Figure 11. The large scattering of the measured pit initiation potential data shown in Figure 11 is typical for passive alloys.

Corrosion Potential. Figure 12 shows the corrosion potentials defined as the potentials at which the net current is zero on the CPP curves.[(2)] The values in Figure 12 were obtained in the different cells for the two types of SS electrodes during the experiment. The corrosion potentials are between –0.37 to –0.15 V_{SCE} for the Type 304L SS electrodes and –0.43 to –0.23 V_{SCE} for the Type 304 SS electrodes in all the three cells. In general, the

[(2)]ASTM Designation: G3–89 (Reapproved 1999), "Standard practice for Conventions Applicable to Electrochemical Measurements in Corrosion Testing" (1999).

corrosion potentials of the test cell are slightly lower than those measured in the control and aerated cells, which is in agreement with the observation for Types 304L and 316 and 316L SS by Ringas and Robinson.[17] It appears that the corrosion potentials measured from the three cells all decreased over time, which was probably due to the increase in solution pH (6.2 at the beginning for all cells and 8.8 for the test, 8.3 for the control and 10.3 for the aerated cells at the end of the test).

Open Circuit Potential. Figure 13 shows the open circuit potentials (the steady-state rest potentials measured prior to the potentiodynamic polarization scans) obtained in the different cells for the two types of SS electrodes. As expected, the open circuit potentials measured in the aerated cell are significantly higher than those obtained in the other two cells because the other two cells were deaerated during the test. Similarly to the observation made by Ringas and Robinson,[17] open circuit potentials measured from the test cell for the two types of SS are consistently lower than those measured in the control cell even though both cells were deaerated using the same high purity nitrogen. This difference is much larger than the values that would be caused by the slight difference between the pH in the two cells (8.3 in the control cell and 8.8 in the test cell). However, no apparent correlation between the SRB density and the open circuit potential of the SS electrodes can be drawn from Figures 13 and 8.

Anodic Currents. As discussed above, the typical anodic behavior observed below the pit initiation potential during the forward potential scan in the test cell is significantly different from that in the other two cells (Figure 9). Anodic currents have been used as criteria to characterize SRB induced corrosion for metals.[17] Other electrochemical methods have been suggested and used for evaluating the susceptibility of metallic materials to MIC and monitoring its occurrence.[18] Therefore, the following values were extracted from the polarization curves obtained in the test cell:

Pit Initiation Current (I_{ip}): The current measured at a potential just below the pit initiation potential.

Mean Passive Current (I_{mean}): The average current for the region between the corrosion potential and the pit initiation potential.

Peak Current (I_{pk}): The peak value as shown in Figure 9.

These values and the SRB density are plotted in Figure 14. It is apparent that all these values, especially the peak current, correlate well with the SRB density. Therefore, they are indications of either a high metal dissolution rate (or corrosion rate) catalyzed by the SRB, as explained by many investigators,[17,19] or a high oxidation rate of certain reducing chemical species that were produced by the SRB in the test cell (see the discussion section).

DISCUSSIONS

The potentiodynamic polarization curves for the Types 304 and 304L SS electrodes show a distinctive anodic peak at potentials above the corrosion potential and significant higher anodic currents for the SRB-containing test cell than for the SRB-free control cell. The anodic galvanic current from the Type 304L SS plate electrode in the SRB-containing test cell coupled to a large SS cathode in the aerated cell is also slightly higher than those obtained in the SRB-free control cell. However, no significant difference was noted between the current signals from the coupled multielectrode array sensor in the test cell and that in the control cell. No difference between the repassivation potentials measured from the two cells were noted either. To understand the nature of the anodic peak and the high anodic current in the test cell when the SRB density was high, potentiodynamic polarization tests were conducted using platinum electrodes. One of the platinum electrodes was placed in the test cell and the other was placed in the control cell at the start of the experiment.

Figure 15 shows that the anodic polarization curves obtained with the platinum electrodes in the two cells near the end of the experiment are similar to those obtained with the SS plate electrodes (Figure 9). No anodic peak was observed with the platinum electrode in the control cell, but a distinctive anodic peak was apparent with

the platinum electrode in the test cell at practically the same potential as the peak found on the SS electrodes. As the dissolution of platinum at the peak potential is unlikely, the peak in Figure 15 is probably due to the oxidation of a chemical species, presumably produced by the SRB. Therefore, it can be concluded that not all the anodic currents discussed above for the SS electrodes (peak current, pit initiation current, and mean passive current) were due to the anodic dissolution. Instead, at least a fraction of each measured current value was due to the oxidation of chemical species produced by the presence of the SRB in the test cell. The correlation between these currents and the SRB density indicates that the amount of the reducing chemical species is proportional to the SRB density.

Figure 16 shows the effect of time interval between the potentiodynamic scans on the anodic polarization peak obtained with the platinum electrode in the test cell near the end of the experiment. The peak current was about 1×10^{-4} A/cm^2 for the initial potentiodynamic polarization test conducted after the electrode was in the SRB-containing solution for three months, whereas the peak current obtained 2 days after the first potentiodynamic polarization test was less than 1×10^{-5} A/cm^2. The peak disappeared in the third scan that was conducted 5 minutes after the completion of the second scan. Figure 16 seems to suggest that the anodic peak is due to the oxidation of a reducing chemical species accumulated on the surface of the platinum electrode by adsorption or chemical reaction over a considerable length of time in the presence of SRB. The peak disappeared in the third scan because the species attached to the surface of the platinum electrode was completely oxidized during the second scan and did not have enough time to accumulate before the start of the third scan.

Figure 17 shows the effect of time interval between the potentiodynamic scans on the anodic peak of the polarization curve obtained with a Type 304L SS electrode in the test cell near the end of the experiment. Same as in Figure 16, the peak is high in the first initial potentiodynamic polarization scan that was conducted 7 days after a previous potentiodynamic polarization scan on the same electrode. The peak disappeared in the second scan that was conduced 15 minutes after the completion of the first scan. Figures 16 and 17 seems to suggest that the anodic peaks as shown in Figures 9 and 17 were at least partially due to the oxidation of a reducing chemical species (or specie) which was accumulated on the surface of the SS electrode in the presence of SRB. Additional work is needed to identify the chemical species that causes the increase in the anodic peak current. Adsorbed sulfur or sulfides are suspected to be responsible for the peak currents because of their presence in the stability diagram.[2,20]

The slightly higher galvanic current obtained with the Type 304L SS electrode in the test cell than in the control cell was probably also due to the oxidation of the reducing species produced by the SRB.

The experimental measurements showed that the presence of SRB in the test cell appears to lower the pit initiation potential, but did not change the repassivation potential of the Types 304 and 304L SS under the test conditions.

The measurement of non-uniform corrosion currents using coupled multielectrode array sensors showed that there was no more localized corrosion for the SS in the SRB-containing sodium chloride solution than in the SRB-free sodium chloride solution. This is probably due to the fact that the electrochemical potential of the SS electrodes was still too low in both environments to initiate localized corrosion. Even though they were coupled to large SS cathodes in the aerated cell and the potentials were maintained between –0.05 to –0.25 V_{SCE} for the Type 304 and –0.04 to –0.235 V_{SCE} for the Type 304L electrodes, these potentials were too low compared to the measured repassivation potentials (–0.01 to –0.15 V_{SCE} for the Type 304 SS and –0.065 to 0.06 V_{SCE} for the Type 304L SS) to cause localized corrosion in the relative short-term test and much lower than the pit initiation potential. Higher potentials are required to initiate and sustain localized corrosion under the test conditions. Such higher potentials may be obtained by the coupling of the SS electrode in the reducing environment to a remote cathode that is exposed to solutions containing oxidizing species such as H_2O_2 and ferric ion, or oxidizing bacteria.

The observation of pitting reported by Rao and Satpathy[21,22] for SS exposed to SRB-containing solutions were not reproduced in this work. The open circuit potentials of the SS specimens were maintained between –0.13

to –0.43 V_{SCE} in the work by Rao and Satpathy and below –0.30 $V_{SCE,}$ in the work by Ringas and Robinson. Both experiments employed semi-continuous mode of SRB growth. The medium used in the test by Ringas and Robinson did not contain dissolved iron. They noted pitting corrosion on Types 304L, 316 and 316L SS specimens after a four-month exposure at 30ºC. Rao and Satpathy noted pitting corrosion on a Type 304 SS specimen after a 25-day exposure. Neither chloride nor slime former (*Vibrio natriegens*) was added in the test solutions used by these investigators. It is not clear if the slime former or the slight difference in the media caused any corrosion inhibition in the present study. Additional tests are continuing to investigate the effect of the addition of the slime former and the media.

The lower open circuit potential and corrosion potential in the SRB environment were attributed to the more active behavior of the alloy in the SRB environment.[17] Because of the presence of reducing chemical species, the reducing species may also contribute to the measured low open circuit and corrosion potentials for the Types 304 and 304L SS electrodes in the presence of SRB.

CONCLUSIONS

Coupled multielectrode array sensors and other electrochemical techniques were used to study the corrosion behavior of Types 304 and 304L SS specimens in 0.5 M NaCl solutions with and without the presence of SRB (*Desulfovibrio vulgaris*). A slime former (*Vibrio natriegens*) was added to the solutions to promote the formation of biofilm. The repassivation potentials were found to be –0.01 to –0.15 V_{SCE} for the Type 304 SS and –0.065 to 0.06 V_{SCE} for the Type 304L SS. No significant difference was observed in the repassivation potentials measured with and without the presence of SRB.

The sensing electrodes of two Type 304 SS coupled multielectrode array sensors and two additional Type 304L plate electrodes in the test solutions were coupled to large SS cathodes in a separate aerated cell and their potentials were increased stepwise from –0.26 to –0.05 V_{SCE} for the sensing electrodes and from –0.25 to –0.04 V_{SCE} for the plate electrodes in approximately a three-month period. No pitting was observed on either the sensing or the plate electrodes. No significant difference between the sensor signals for localized corrosion was observed with and without the presence of SRB.

It was found that each of the anodic polarization curves obtained in the SRB-containing test cell has a distinctive current peak and the current values of the anodic curves were significantly higher than those obtained in the SRB-free control cell. As a general trend, the anodic curves were found to increase with the increase in the cell density of the SRB in the solution.

Anodic polarization measurements using a platinum electrode in the same SRB-containing solution showed the same anodic peak as found on the SS electrodes. It was found that this peak increased with the time interval between the potentiodynamic polarization scans, indicating that the anodic peak could be due to the oxidation of reducing species attached to the electrode surface. Similar effects of the time interval between the potentiodynamic scans on the anodic peak were also observed on the SS electrodes. It can be concluded that use of the anodic current density alone to characterize microbially induced corrosion might lead to misinterpretation.

ACKNOWLEDGMENTS

This paper was prepared to document work performed by the Center for Nuclear Waste Regulatory Analyses (CNWRA) for the Nuclear Regulatory Commission (NRC) under Contract No. NRC–02–02–012. The activities reported here were performed on behalf of the NRC Office of Nuclear Material Safety and Safeguards, Division of Waste Management. This paper is an independent product of the CNWRA and does not necessarily reflect the view or regulatory position of the NRC.

The authors would like to thank Sean Brossia (Southwest Research Institute) for the important contributions to the work presented in this paper at the beginning of the study. The technical assistance by and the discussions with Geri Becker (Applied Becker Consulting) and Stuart Birnbaum (University of Texas at San

Antonio) in the microbial aspects of this work, and the laboratory assistance by Roger J. Dykstra and Brian Derby (Southwest Research Institute) are acknowledged.

REFERENCES

1. D. Thierry and W. Sand, "Microbially Influenced Corrosion," in Corrosion Mechanisms in Theory and Practice, P. Marcus and J. Oudar, eds., Marcel Dekker, Inc., 1995, New York, Chapter 13, p. 457.

2. Multi-author review, "Microorganisms in Nuclear Waste Disposal," *Experientia*, Part I, 46 (1990), pp. 777–851.

3. Multi-author review, "Microorganisms in Nuclear Waste Disposal," *Experientia*, Part II, 47 (1991), pp. 507–583.

4. G. Geesey and G.A. Cragnolino, "A Review of the Potential for Microbially-Influenced Corrosion of High Level Nuclear Waste Containers in an Unsaturated Repository Site," in *1995 International Conference on Microbially Influenced Corrosion,* P. Angell, S.W. Borenstein, R.A. Buchanan, S.C. Dexter, N.J.E. Dowling, B.J. Little, C.D. Lundin, M.B. McNeil, D.H. Pope, R.E. Tatnall, D.C. White, and H.G. Ziengenfuss, eds., Houston, TX: NACE International (1995), pp.76/1–76/20 .

5. U.S. Department of Energy, Yucca Mountain Science and Engineering Report, U. S. Department of Energy, Office of Civilian Radioactive Waste Management, DOE/RW–0539, Las Vegas, NV, May 2001.

6. G.M. Gordon, "Corrosion Considerations Related to Permanent Disposal of High-Level Radioactive Waste," *Corrosion*, 58 (2002), pp.811–825.

7. J. Horn, C. Carrillo and V. Dias, "Comparison of the Microbial Community Composition at Yucca Mountain and Laboratory Test Nuclear Repository Environments," CORROSION/2003, paper no. 03556, (Houston, TX: NACE International, 2003).

8 C.S. Brossia and L. Yang, "Studies of Microbiologically Influenced Corrosion Using a Coupled Multielectrode Array Sensor," CORROSION/2003, paper no. 03575, (Houston, TX: NACE International, 2003).

9. L. Yang and N. Sridhar, "Coupled Multielectrode Online Corrosion Sensor," *Materials Performance*, No. 9 (2003), pp. 48–52.

10. L. Yang, N. Sridhar, O. Pensado and D. S. Dunn, "An *In-Situ* Galvanically Coupled Multielectrode Array Sensor for Localized Corrosion," *Corrosion*, 58 (2002), p. 1,004.

11 L. Yang, N. Sridhar and G. Cragnolino, "Comparison of Localized Corrosion of Fe Ni-Cr-Mo Alloys in Chloride Solutions Using a Coupled Multielectrode Array Sensor," CORROSION/2002, paper no. 02545, (Houston, TX: NACE International, 2002).

12. M. Akashi, G. Nakayama and T. Fukuda, "Initiation Criteria for Crevice Corrosion of Titatium Alloys Used for HLW Disposal Overpack," CORROSION/1998, paper no. 158, (Houston, TX: NACE International, 1998).

13. Y. Yao, K. Masamura, T. Kondo, and Y. Ujiie, "Effect of Iron-Oxidizing Bacteria on the Corrosion Behavior of Type 304 Stainless steel." CORROSION/1999, paper no. 166, (Houston, TX: NACE International, 1998).

14. B.H. Olesen, R. Avci, and Z. Lewandowski, "Ennoblement of Stainless Steel Studied by X-Ray Photoelectron Spectroscopy," CORROSION/1998, paper no. 275, (Houston, TX: NACE International, 1998).

15. K. Ito, R. Matsuhashi, T. Kato, O. Miki, H. Kihira and K. Watanabe, P. Baker, "Potential Ennoblement of Stainless Steel by Marine Biofilm and Microbial Consortia Analysis," CORROSION/2002, paper no. 02452, (Houston, TX: NACE International, 2002).

16. H. Amaya and H. Miyuki, "Laboratory Reproduction of Potential Ennoblement of Stainless Steels in Natural Seawater," CORROSION/1999, paper no. 168, (Houston, TX: NACE International, 1998).

17. C. Ringas and F.P.A. Robinson, "Corrosion of Stainless Steel by Sulfate-Reducing Bacteria-Electrochemical Techniques," *Corrosion*, 44 (1988), pp. 386–396.

18. O.H. Tuovinen and G. Cragnolino, "A Review of Microbiological and Electrochemical Techniques in the Study of Corrosion Influenced by Sulfate-Reducing Bacteria," in Corrosion Monitoring in Industrial Plants Using Nondestructive Testing and Electrochemical Methods, G. C. Moran, P. Labine, eds., (Conshohocken, PA: American Society for Testing and Materials, Special Technical Publication 908, 1986), p. 412–432.

19 B.J. Webster, R.G. Kelly, and R.C. Newman, "The Electrochemistry of SRB Corrosion in Austenitic Stainless Steel," in Microbially Influenced Corrosion and Biodeterioration, Dowling, Mittelman, and Danko, eds., Houston, TX: NACE International (1990), pp. 2.9–2.17.

20. P. Marcus, "Sulfur-Assisted Corrosion Mechanisms and the Role of Alloyed Elements," in Corrosion Mechanisms in Theory and Practice, P. Marcus and J. Oudar, eds., Marcel Dekker, Inc., New York (1995), p. 239.

21. T.S. Rao and K.K. Satpathy, "Studies on Pitting Corrosion of Stainless Steel (SS-304) by a Marine Strain of Sulfate Reducing Bacteria (*Desulfovibrio vulgarious*)," in Microbial Corrosion: Proceedings of the 4th International EFC Workshop, European Federation of Corrosion, Publication No 29, C.A.C. Sequira, ed., London, IOM Communications (2000), p. 79.

22. C. Ringas and F.P.A. Robinson, "Corrosion of Stainless-Steel by Sulfate-Reducing-Bacteria Total Immersion Test-Results," *Corrosion*, 44 (1988), p. 671.

TABLE 1
1.5% NaCl NUTRIENT BROTH

Chemicals	Amount
Beef Extract	3.0 gm
Peptone	5.0 gm
Sodium Chloride	15.0 gm
Distilled Water	1000 mL
Final pH @ 25° C	7.0 ± 0.3

TABLE 2
MODIFIED BAAR'S BROTH MEDIUM

Chemicals	Amount
Sodium Chloride	5 gram
Sodium Citrate	5 gram
Magnesium sulfate	2 gram
Ammonium Chloride	1 gram
Calcium Sulfate	1 gram
Potassium Phosphate (Dibasic)	0.5 gram
Sodium Lactate (60 %wt)	3.5 mL
Yeast Extract	1 gram
Ferrous Ammonium Sulfate	1 gram
Distilled Water	1,000 mL
Final pH at 25 ^{o}C	6.5 ± 0.3

TABLE 3
CHEMICAL COMPOSITIONS (%WT) OF THE SS MATERIALS USED IN THE EXPERIMENT

Metals	UNS #	Ni	Cr	Fe	Mo	Mn	Si	Cu	P	S	C
304 SS	S30400	9.16	18.5	Bal*	0.38	1.10	0.33	0.27	0.019	0.006	0.030
304L SS	S30403	8.29	18.3	Bal	0.4	1.36	0.43	0.26	0.03	0.01	0.02

*Bal: Balance

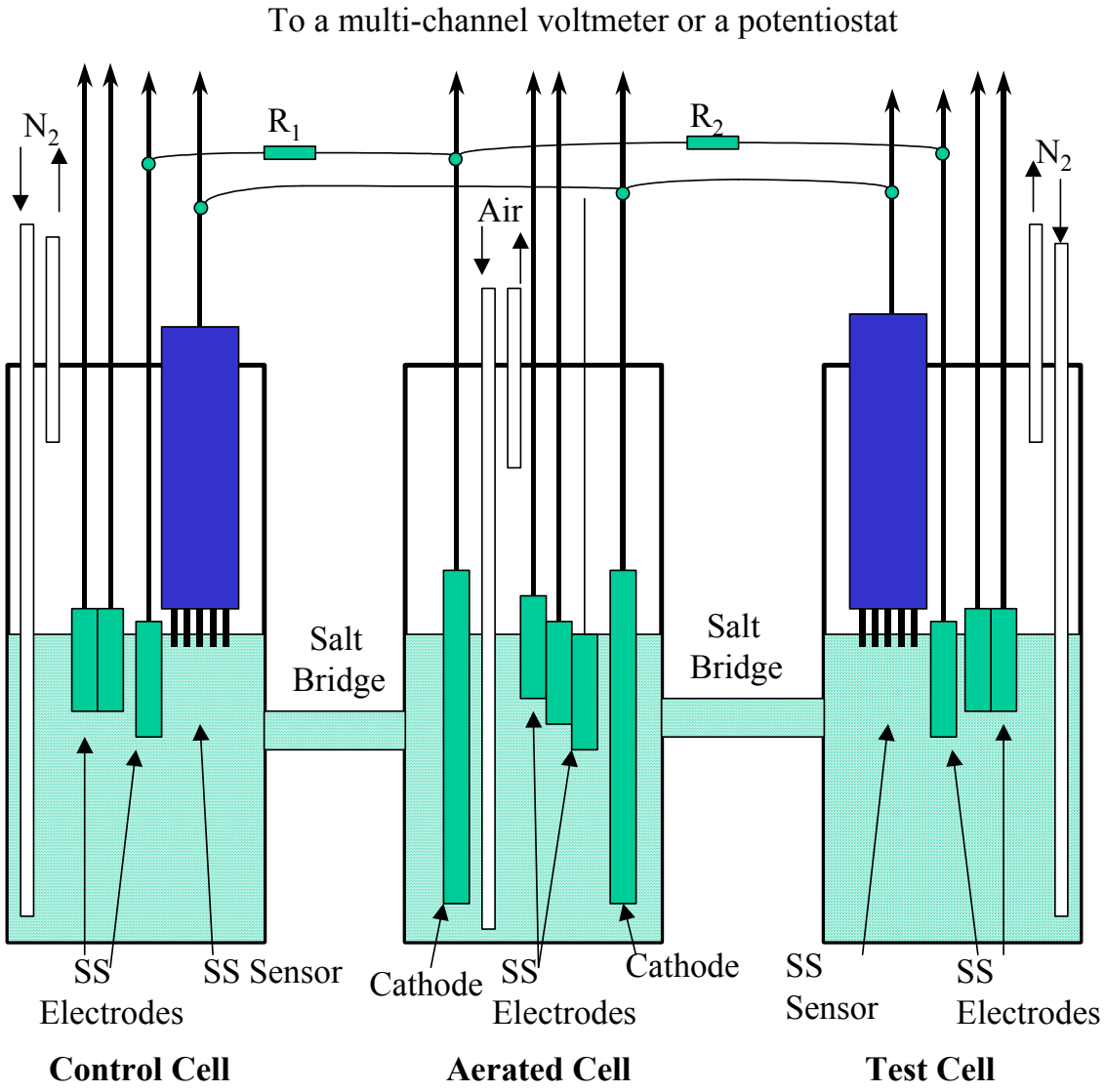

FIGURE 1. Schematic diagram of the experimental setup. Reference and platinum electrodes are not shown. R_1 and R_2 are the resistors for the measurements of the galvanic coupling currents to a cathode. The second cathode was connected to the common joints of the SS sensing electrodes of the two sensors.

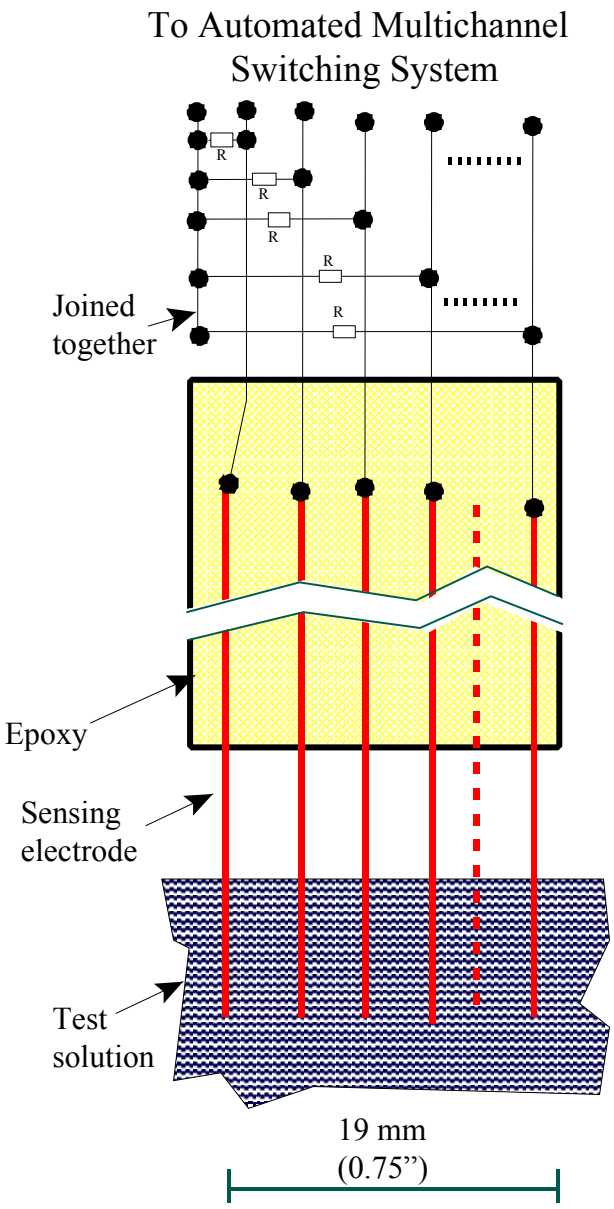

FIGURE 2. Schematic diagram of a crevice-free coupled multielectrode array sensor

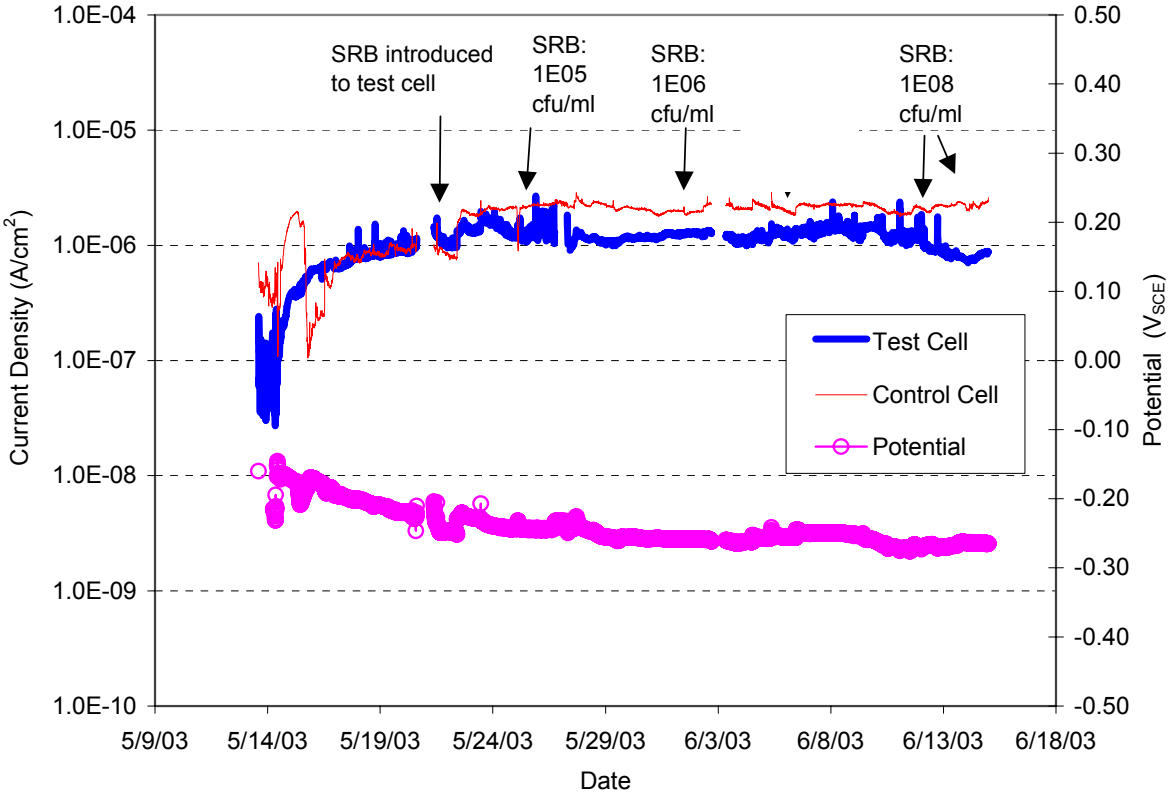

FIGURE 3. Non-uniform current signals from the coupled multielectrode array sensors made of Type 304 SS and the potential during the first 30 days of a test

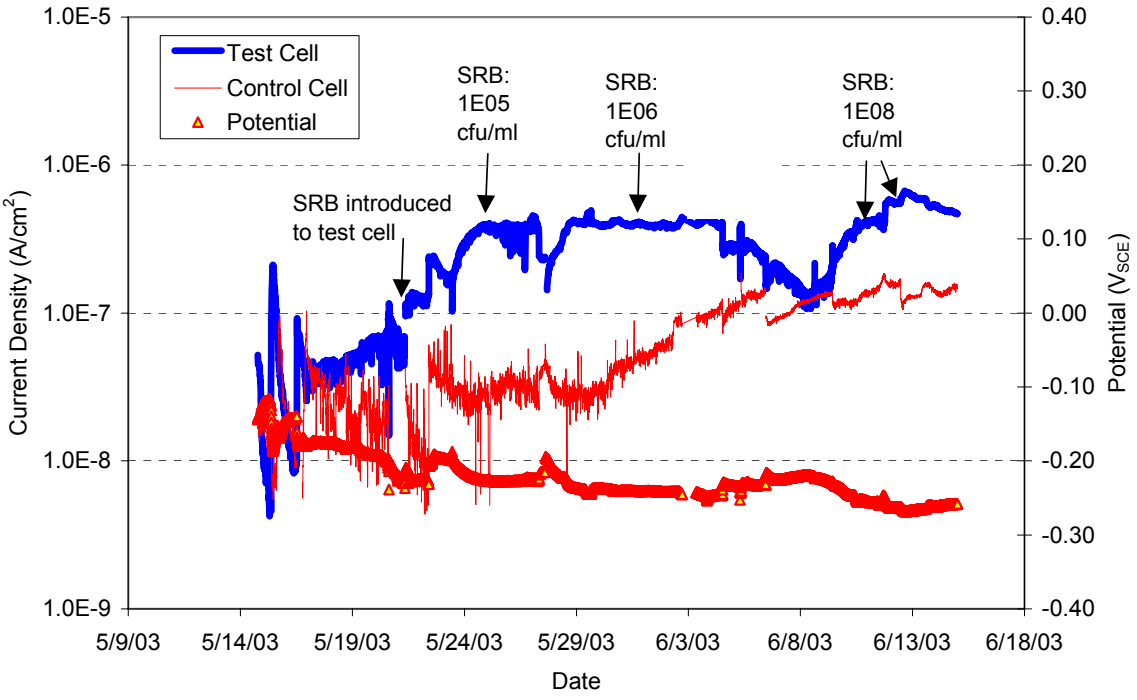

FIGURE 4. Galvanic coupling currents from the Type 304L SS plate electrodes and the potential during the first 30 days of a test

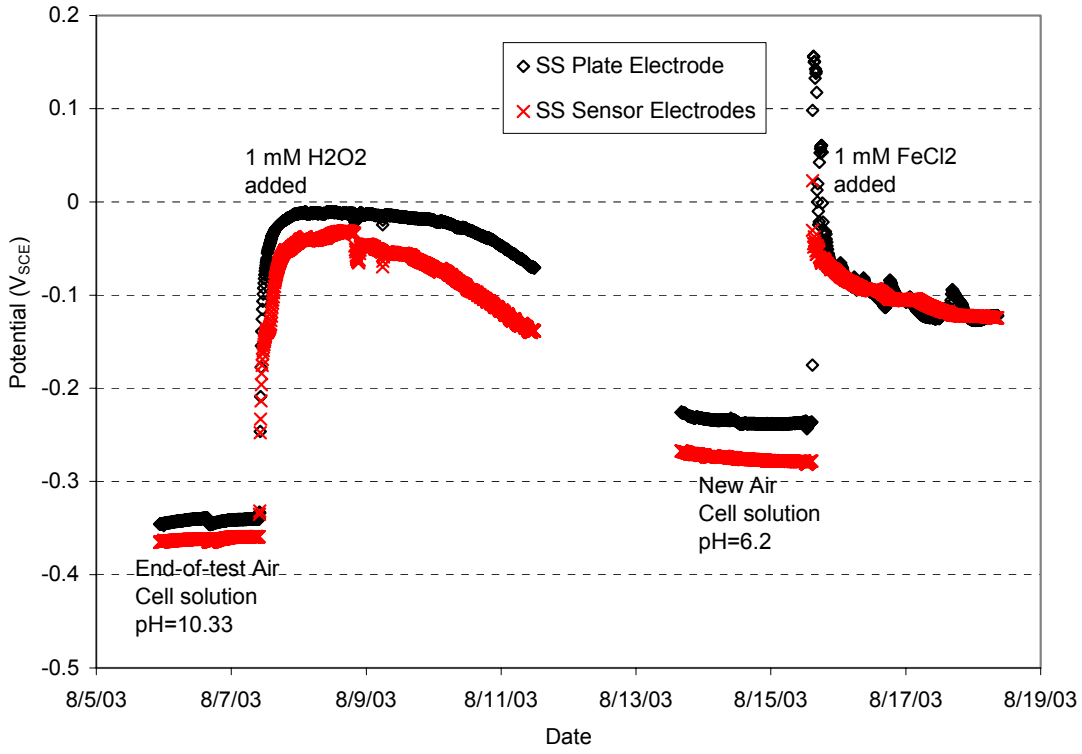

FIGURE 5. Responses of potentials of the sensors and the SS plate electrodes to the additions of H_2O_2 and $FeCl_2$ to the aerated cell

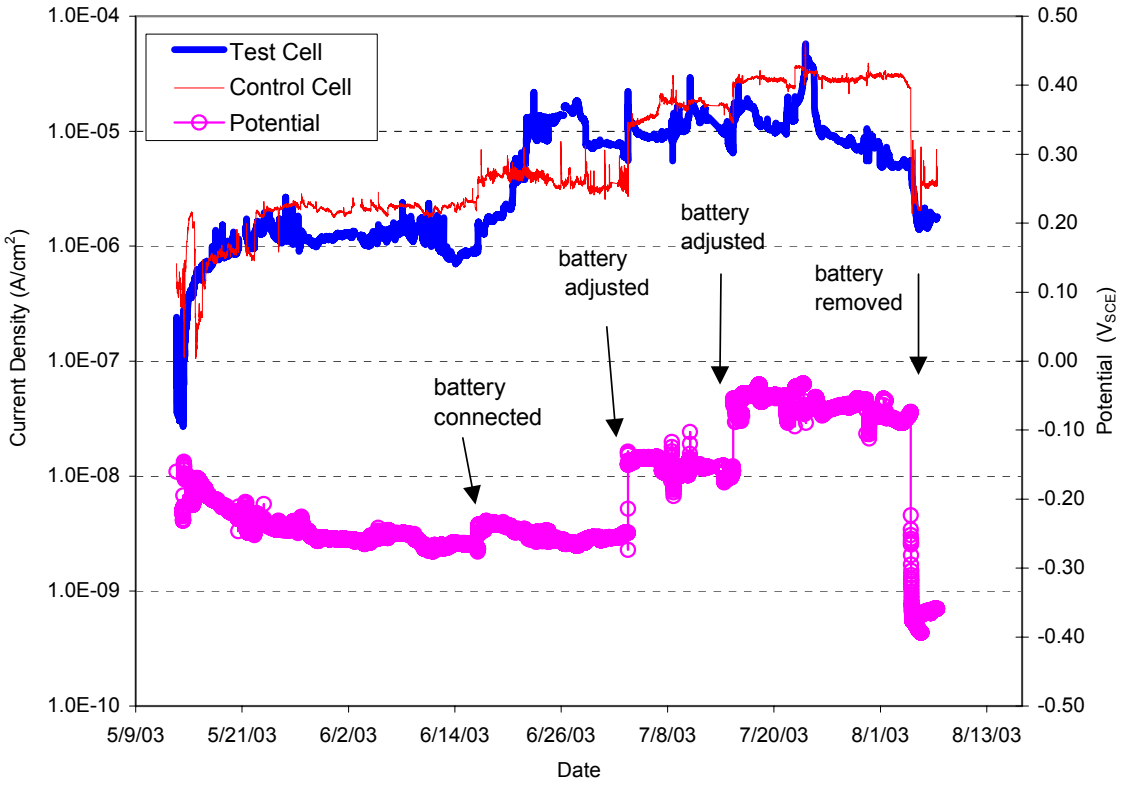

FIGURE 6. Responses of non-uniform currents of the coupled multielectrode array sensors to the changes of the coupling potential

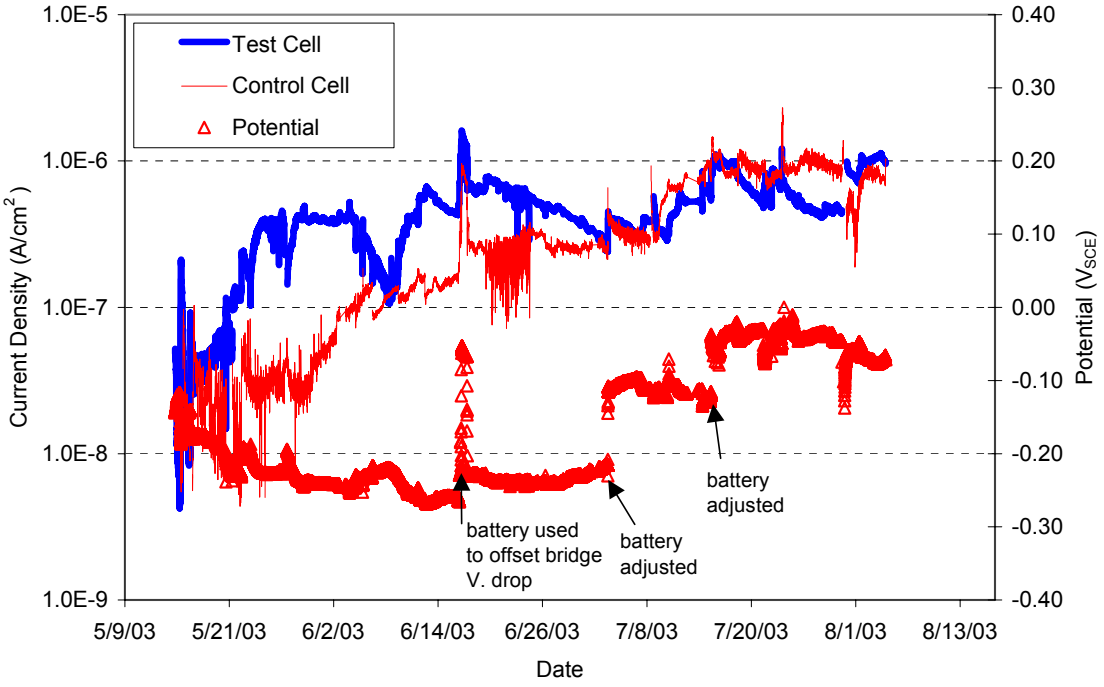

FIGURE 7. Responses of the galvanic coupling currents of the SS plate electrodes to the changes of the coupling potential

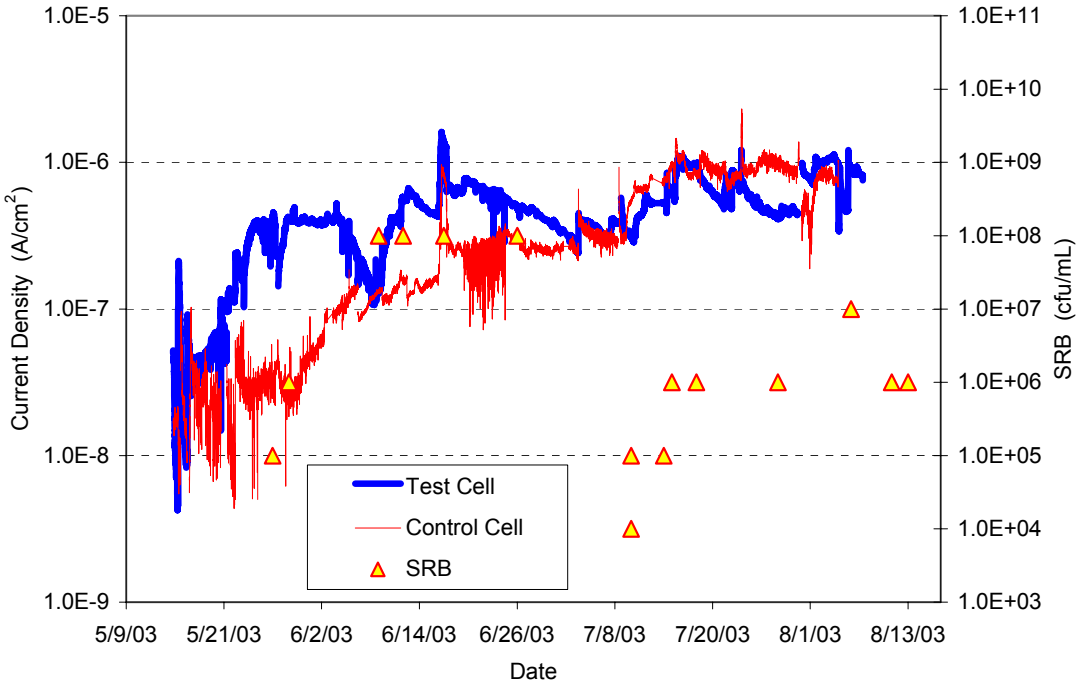

FIGURE 8. Galvanic coupling currents and SRB density during the experiment as indicated in Figure 7. SRB dropped on 6/26 due to the interruption of medium addition .

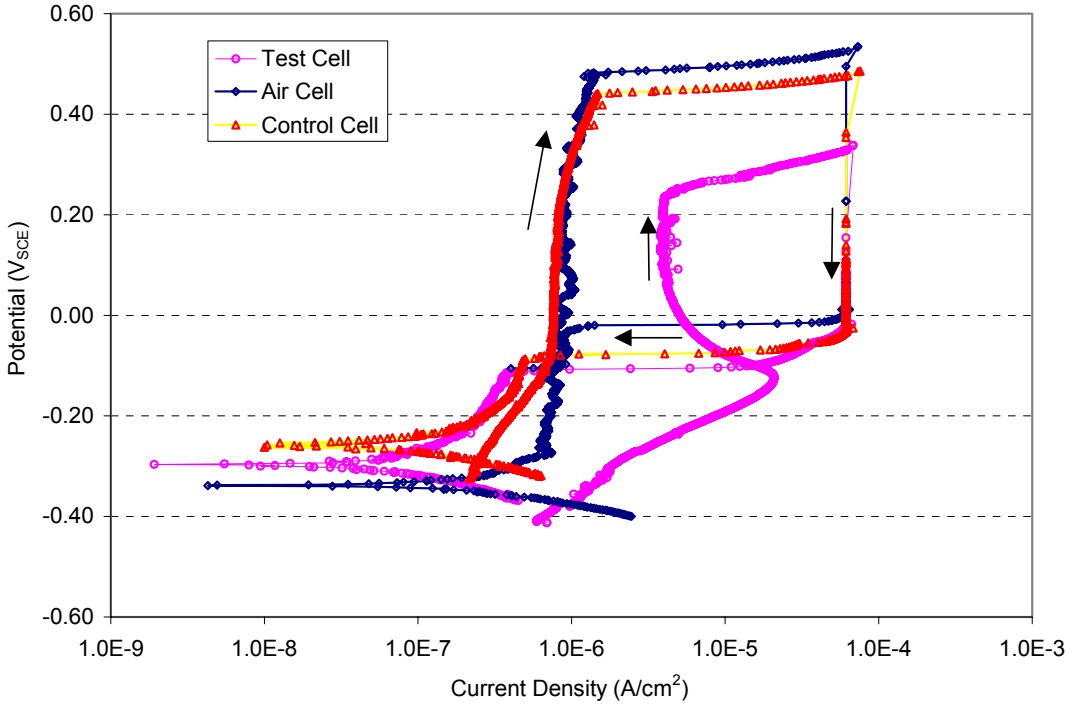

FIGURE 9. Typical cyclic potentiodynamic polarization curves obtained in the different electrochemcial cells for Types 304 and 304L SS

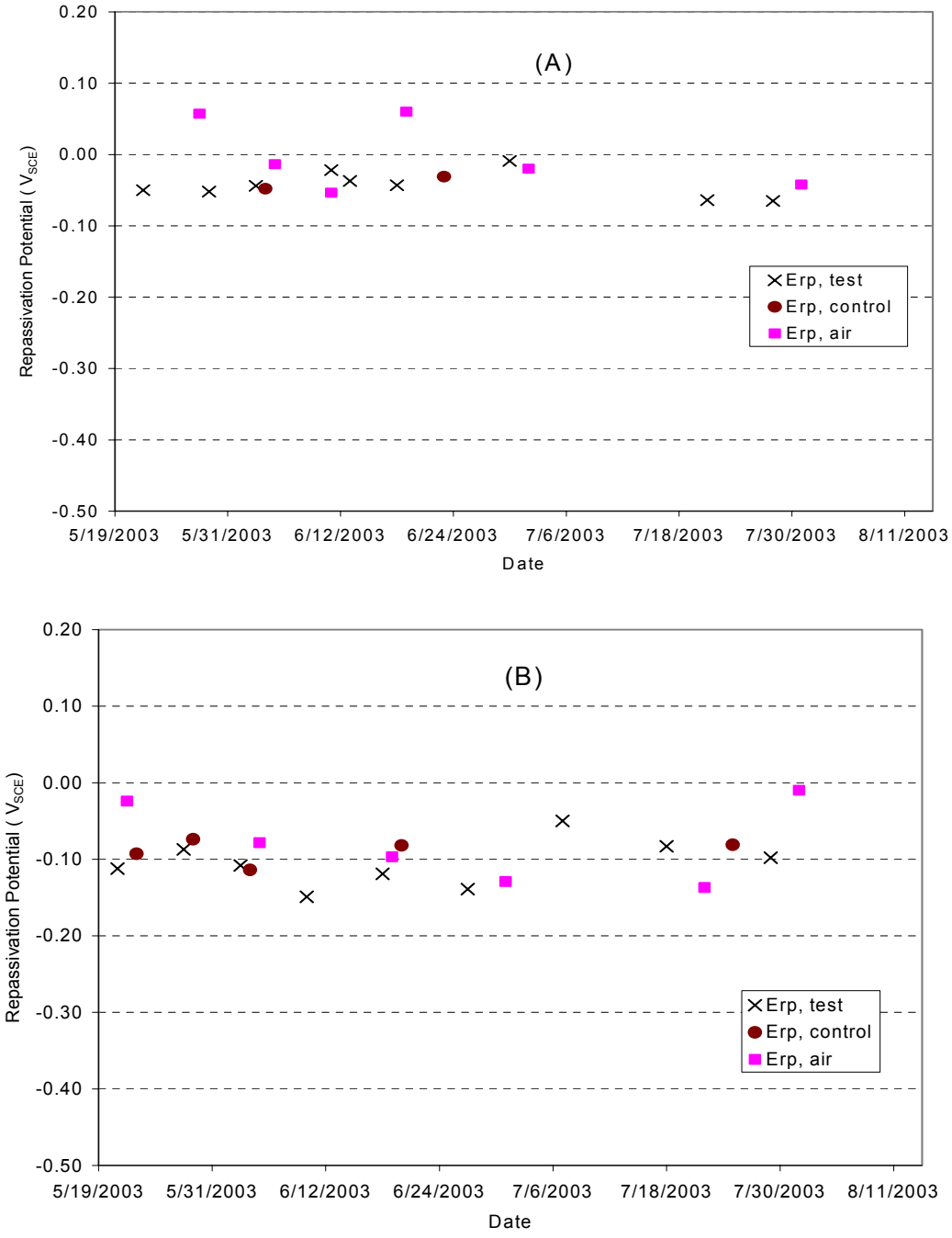

FIGURE 10. Repassivation potentials of Types (A) 304L and (B) 304 SS electrodes

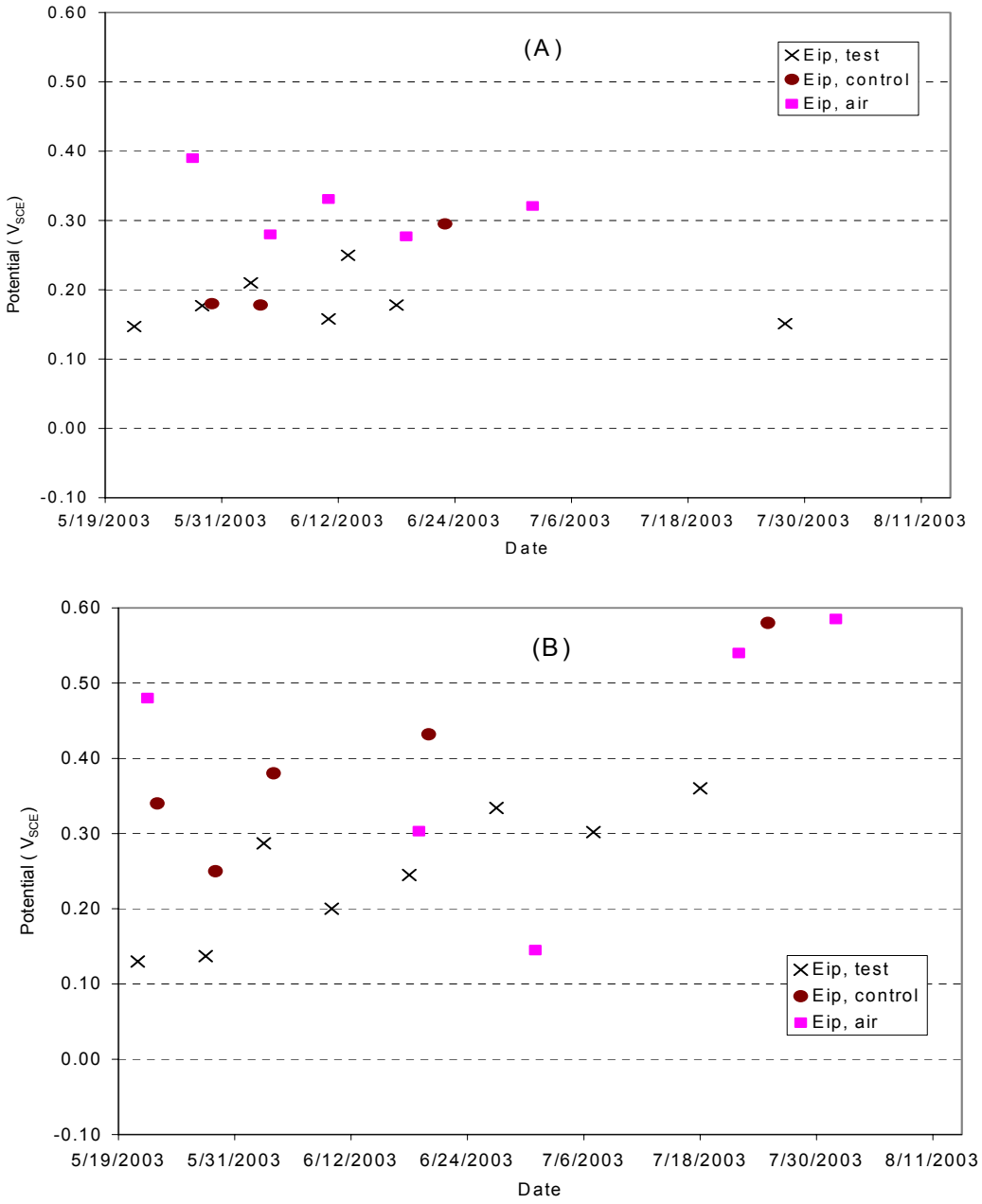

FIGURE 11. Pit initiation potentials for Types (A) 304L and (B) 304 SS electrodes

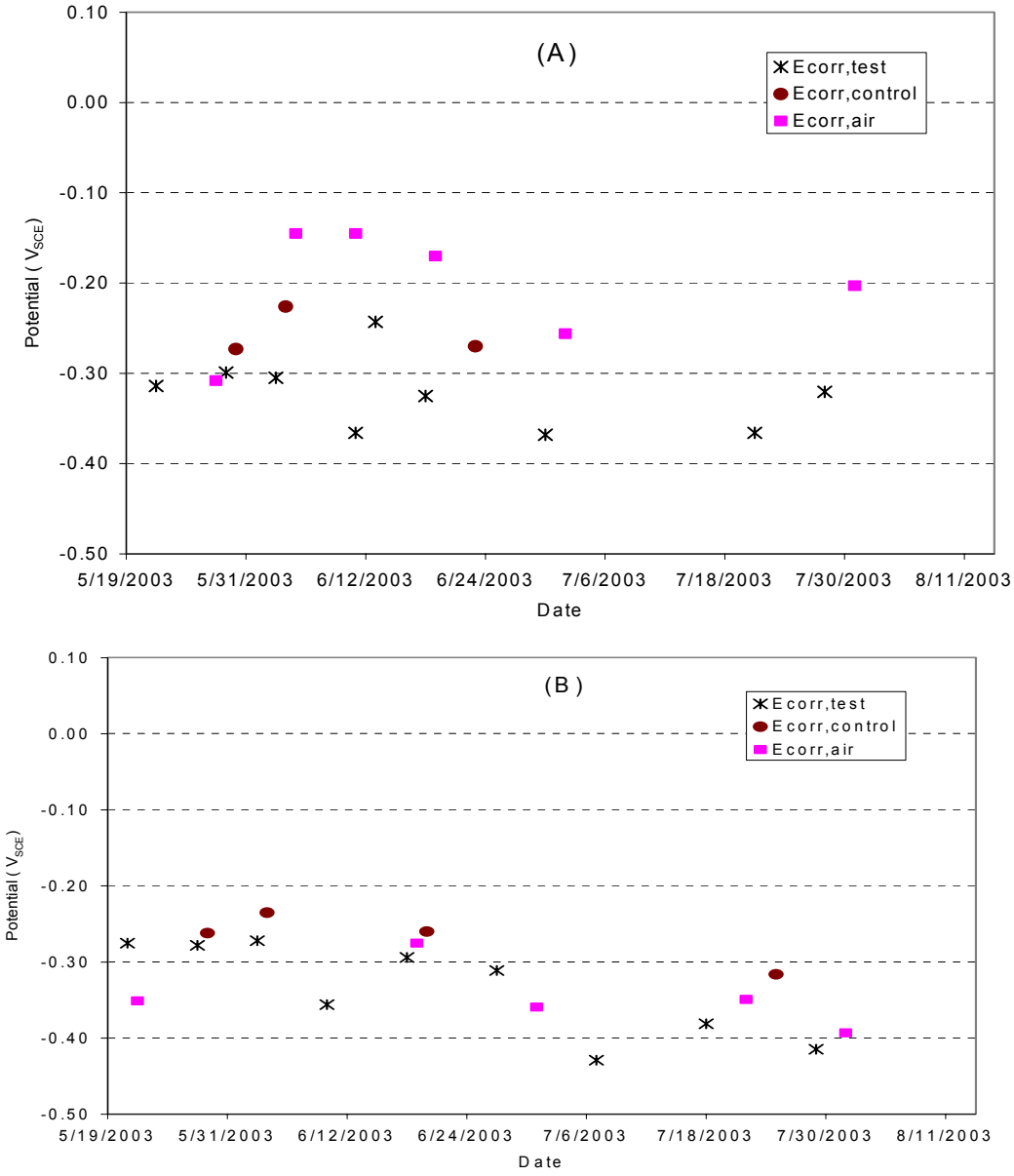

FIGURE 12. Corrosion potentials for Types (A) 304L and (B) 304 SS electrodes

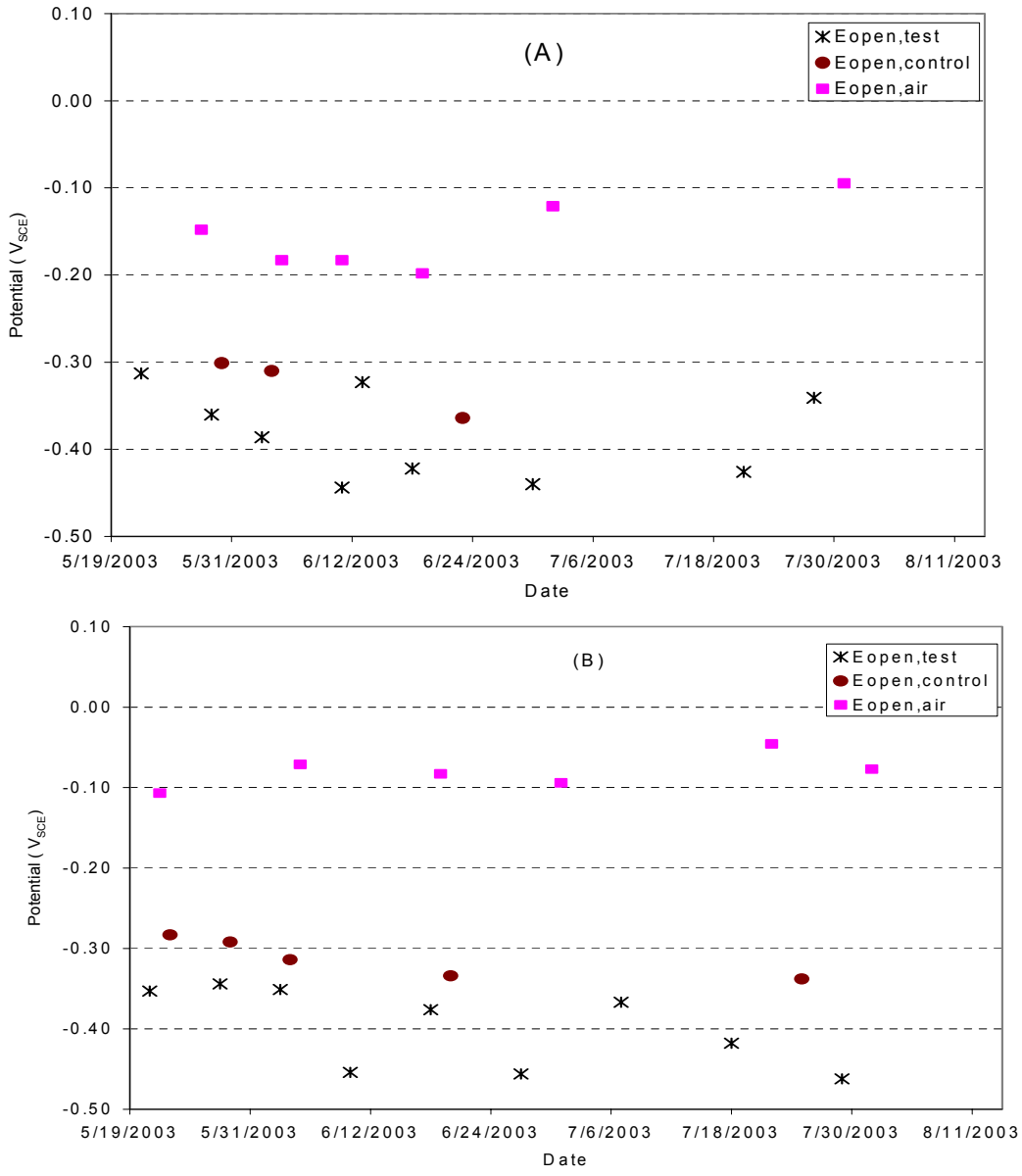

FIGURE 13. Open circuit potentials for Types (A) 304L and (B) 304 SS electrodes

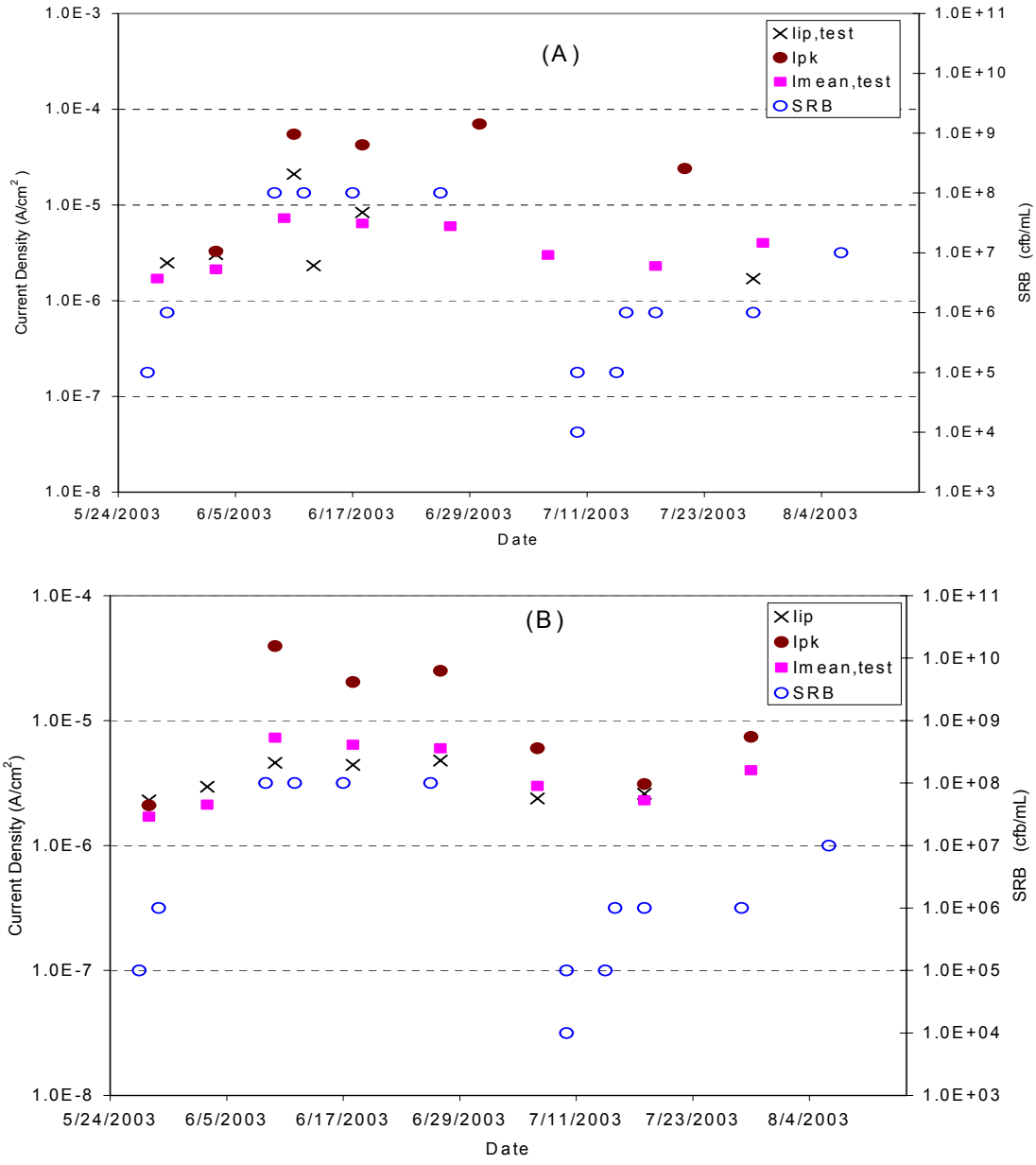

FIGURE 14. Anodic polarization currents below the pit initiation potentials for Types(A) 304L and (B) 304 SS electrode

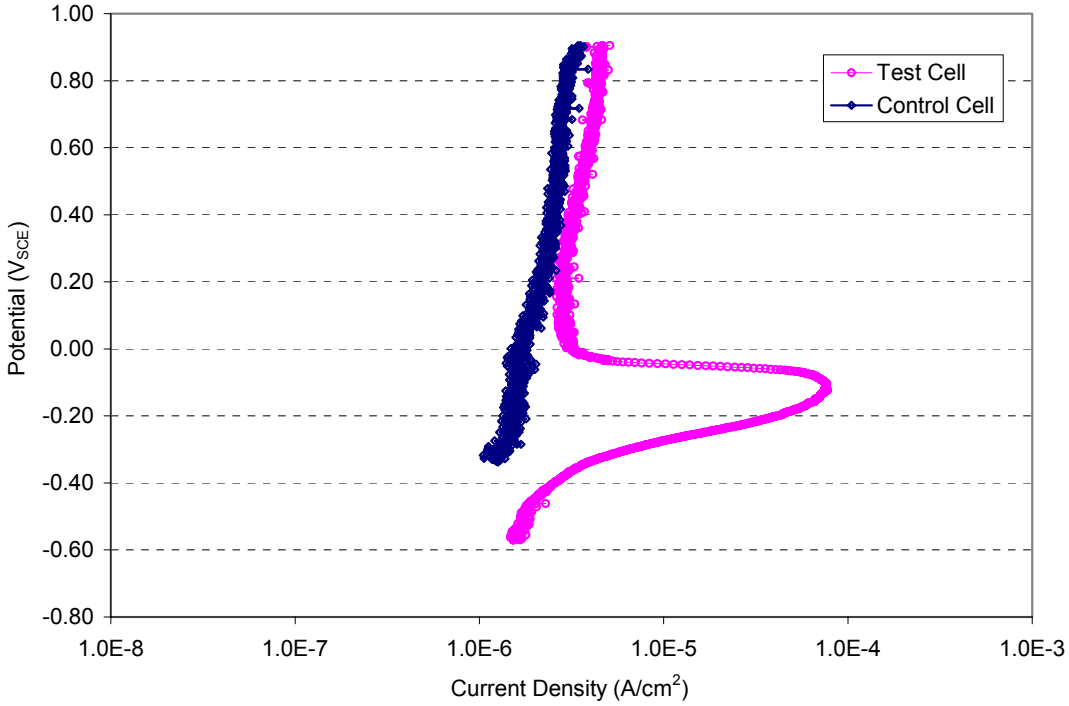

FIGURE 15. Differences between the typical anodic polarization curves obtained with platinum electrodes in the test and in the control cells

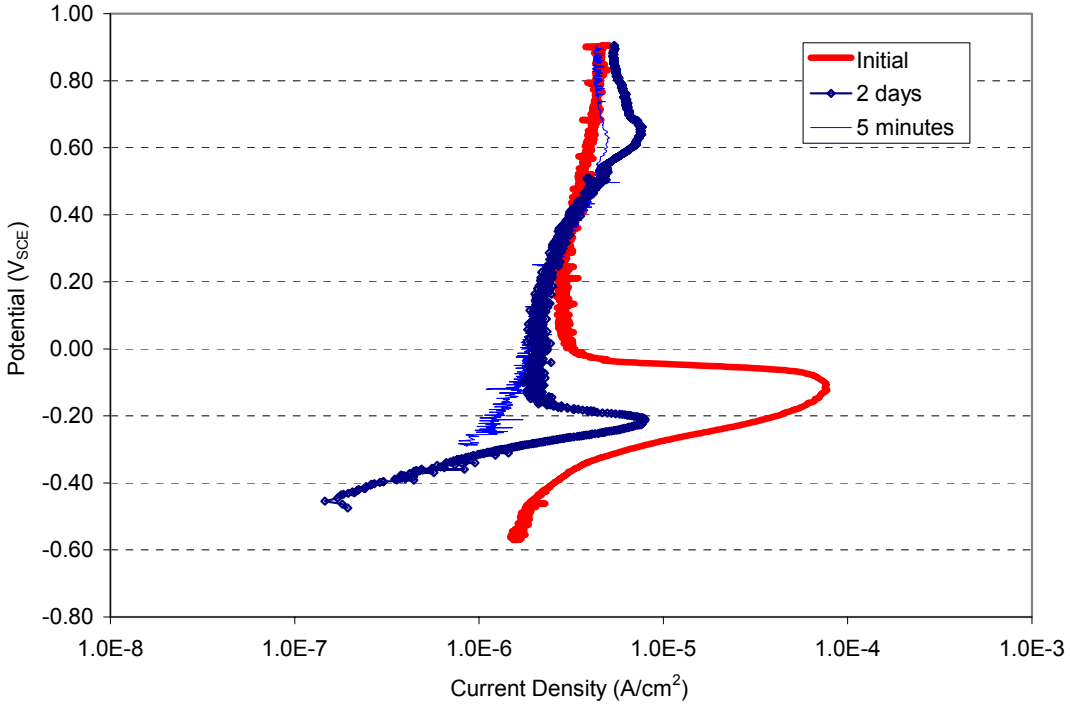

FIGURE 16. Effect of time interval between potentiodynamic polarization scans on the anodic peaks of the polarization curves obtained with a platinum electrode. The initial scan was conducted after the electrode was in the solution for 3 months.

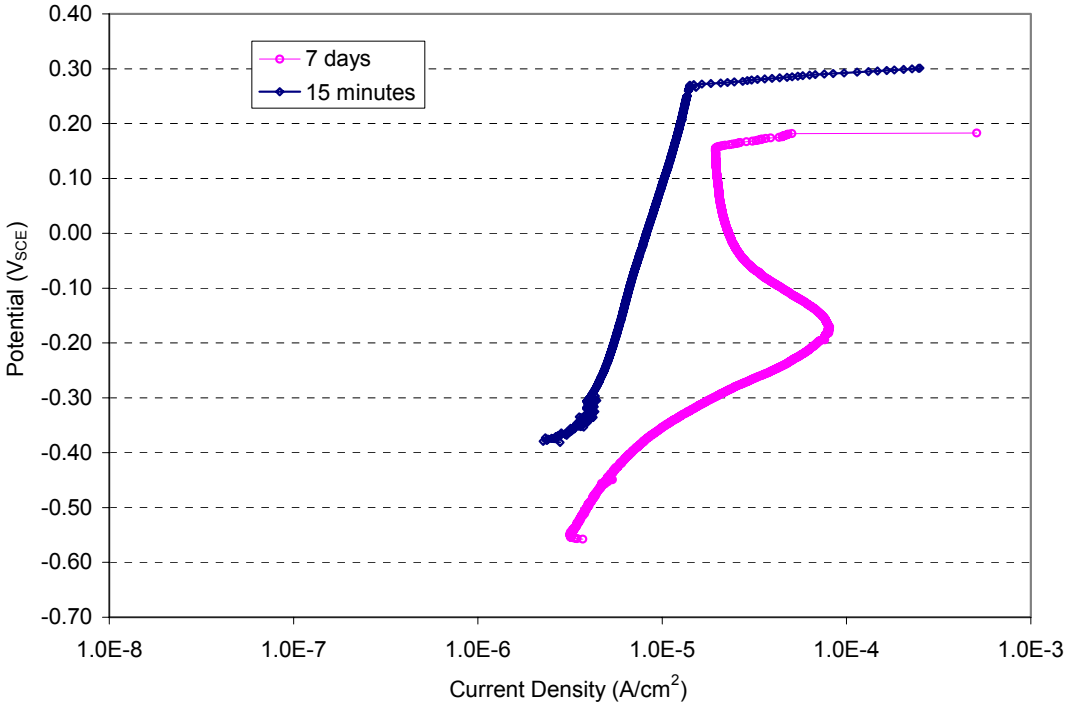

FIGURE 17. Typical effect of time interval between potentiodynamic polarization scans on the anodic peaks of the polarization curves obtained with an SS electrode